JOURNAL OF SOLID STATE CHEMISTRY **131,** 326–334 (1997)
ARTICLE NO. SC977388

Synthesis and Crystal Structure of the Pseudo-Hollandite $Rb_{0.62}Cr_5Te_8$ and Analysis of the Electronic Band Structures of the $Rb_xCr_5Te_8$ Phases

Florent Boucher, James Gareh, Olivier Gourdon, and Michel Evain[1]

Laboratoire de Chimie des Solides, I.M.N., UMR C6502 CNRS, Université de Nantes, 2 rue de la Houssinière, B.P. 32229, 44322 Nantes Cedex 3, France

and

C. J. O'Connor

Department of Chemistry, University of New Orleans, New Orleans, Louisiana 70148

Received October 14, 1996; in revised form March 6, 1997; accepted March 11, 1997

Pseudo-hollandite $Rb_{0.62}Cr_5Te_8$ was prepared from Rb_2Te and elemental Cr and Te at 850°C. Its crystal structure was refined from single crystal X-ray diffraction data. $Rb_{0.62}Cr_5Te_8$ crystallizes in the monoclinic system, $C2/m$ space group, with $a = 20.367(8)$, $b = 3.902(2)$, $c = 9.605(3)$ Å, and $\beta = 104.386(9)°$, $V = 739.3(8)$ Å^3, and $Z = 2$. The structure determination was carried out on 1404 reflections ($I > 3\sigma(I)$) and refinement of 47 parameters yielded the reliability factors $R = 2.57\%$ and $R_w = 2.79\%$. The structure of pseudo-hollandite $Rb_{0.62}Cr_5Te_8$ is analogous to the $TlCr_5Te_8$ structure, which differs from that of hollandite $Rb_{0.73}Cr_5Te_8$. An analysis of the electronic band structures of pseudo-hollandite $Rb_{0.62}Cr_5Te_8$ and hollandite $Rb_{0.73}Cr_5Te_8$, calculated by means of the self-consistent *ab initio* tight-binding linear-muffin-tin-orbital method in the atomic sphere approximation, is presented. Spin-polarized calculations indicate that the $Rb_xCr_5Te_8$ phases are not half-metallic ferromagnets. The rubidium nonstoichiometry and the $Rb_xCr_5Te_8$ relative stability are also discussed.

INTRODUCTION

The binary chromium phases Cr_xX_y (X = S, Se, Te) have been extensively studied for their remarkable magnetic properties, those properties continuously changing from antiferromagnetic for the sulfides to ferromagnetic for the tellurides. The calculation of their electronic structures gave a coherent picture of the changes generated by the anion substitution (1). A closely related compound, $KCrSe_2$, was first reported (2a) as a half-metallic ferromagnet, that is a compound which is metallic for one spin direction and semiconducting for the other spin direction (2b). Recently it was, however, clearly identified as a simple semiconductor (2c). In view of those interesting results and of our discovery of a new phase, $Rb_{0.73}Cr_5Te_8$ (3), we decided to investigate the $Rb_xCr_5X_8$ chromium ternary phases.

Various studies have described the preparation and the crystal structure of the family of materials AM_5X_8 (A = alkali metals, Cd, Sn, Pb, Tl; $M = V$, Cr, Ti; X = S, Se, Te) (4). These materials can be described as having a pseudo-hollandite structure consisting of a M_5X_8 skeleton forming channels in which the alkali or ternary metal is held. Previous preparations of the alkali metal intercalated chromium tellurides have been carried out via ion exchange of the thallium compound $TlCr_5Te_8$, itself being prepared from the elements. It was felt that this preparative route was not ideal due to the inherent nature of ion exchange (i.e., complete exchange of ions within the material is difficult to achieve due to kinetic restraints). For this reason the direct preparation from the elements (or binary precursors) was attempted. Initially the material $Rb_{0.73}Cr_5Te_8$ previously mentioned was prepared directly from the elements in a sealed silica tube and resulted in a slightly different structural type, more closely related to that of the true hollandite material (3).

In this paper we first report the preparation and the structure determination of the material $Rb_{0.62}Cr_5Te_8$, with a structure analogous to the "pseudo hollandites," that is that of $TlCr_5Te_8$. Then we present a comparative study of the electronic band structures of both phases, $Rb_{0.73}Cr_5Te_8$ and $Rb_{0.62}Cr_5Te_8$, calculated by means of the self-consistent *ab initio* tight-binding linear-muffin-tin-orbital method in the atomic sphere approximation (TB-LMTO-ASA).

1. EXPERIMENTAL

Synthesis. Due to the difficulty of handling rubidium metal at room temperature, an alloy of rubidium and

[1] To whom correspondence should be addressed.

0022-4596/97 $25.00

tellurium was first prepared. Elemental rubidium and tellurium were mixed in liquid ammonia (Rb, 0.12 g, 1.4 mmol; Te, 0.09 g, 0.7 mmol) and this more stable product (of approximate stoichiometry Rb_2Te) was used for subsequent reaction.

Preparation of the target material $RbCr_5Te_8$ was attempted by direct reaction of the rubidium tellurium alloy (0.064 g, 0.2 mmol), chromium (0.105 g, 2.0 mmol), and tellurium (0.387 g, 3.0 mmol) in an evacuated sealed silica tube. The tube was heated at a rate of 15°C/hr to 850°C and after a period of 5 days cooled at a rate at of 10°C/hr to room temperature.

Semi-quantitative analyses of the resulting black material by means of a JEOL microscope (TRACOR-TN 5500 equipped JEOL-JSM35C) indicated the presence of crystals of both the binary material Cr_2Te_3 and a ternary material with an approximate stoichoimetry of $Rb_{0.8}Cr_5Te_{8.1}$.

Single crystal studies. Single crystals were extracted from the bulk both in an atmosphere of argon and in air. It was found that the ternary crystals were air-stable and thus all subsequent crystal manipulations were carried out in air. Weissenberg photographs were used to determine the quality of the crystals and also their nature (either Cr_2Te_3 or the ternary $Rb_xCr_5Te_8$) and the best ternary crystal was used for data collection on a Nonius CAD4-F diffractometer (MoK-$L_{2,3}$ radiation). The recording conditions are reported in Table 1.

The data were treated for Lorentz and polarization effects and a Gaussian absorption correction was carried out using the XTAL program package (6). Equivalent reflections were averaged according to the $2/m$ Laue symmetry ($R_{int} = 2.71\%$ on intensity), yielding 1404 independent hkl with $I > 3\sigma(I)$ for subsequent refinement. See Table 1 for details.

Structure refinement. All structure refinements were carried out using the SDS95 program package (7) and atomic scattering factors for neutral atoms with corrections for anomalous dispersion were taken from the literature (8). Initial atomic positions were taken from the proposed structure of $TlCr_5Te_8$ (4j). Full matrix refinements in the space group $C2/m$ with full occupancy for all atoms yielded a reliability factor of $R = 3.75\%$ ($R_w = 6.10\%$). A Fourier difference map analysis then revealed a large positive peak at the rubidium site (7.07 e Å^{-3}), surrounded by negative residues (-5.1 e Å^{-3}). These residues, along with relatively large atomic displacement parameters (ADP) for rubidium implied a partial occupancy of the rubidium site. Refinement of the rubidium occupancy led to a chemical occupancy of 0.619(6) and a decrease in both the reliability factors $R = 2.57\%$ ($R_w = 2.79\%$) and the corresponding ADPs. The resulting electron density residues became featureless. The refined atomic site parameters are given in Table 2.

TABLE 1
Crystallographic Data for $Rb_{0.62}Cr_5Te_8$

Physical, crystallographic, and analytical data			
Formula		$Rb_xCr_5Te_8$, $x = 0.619(6)$	
Molecular weight (g mol^{-1})		1333.8	
Crystal system		Monoclinic	
Space group		$C2/m$ (No. 12)	
Cell parameters (from 25 reflections; $\theta = 10$–25):			
a (Å)	20.367(8)		
b (Å)	3.902(2)	β(°)	104.386(9)
c (Å)	9.605(3)		
V (Å^3)	739.3(8)	$Z = 2$	
Density calc. (g cm^{-3})		5.989	
Data collection			
Temperature (K)		293	
Diffractometer		CAD4-F	
Radiation		MoK-$L_{2,3}$ (0.71073 Å)	
Crystal color		Black (metallic luster)	
Crystal description		Platelet	
Crystal size (mm^3)		$\approx 0.11 \times 0.05 \times 0.015$	
Linear absorption coeff. (cm^{-1})		209.44	
Monochromator		Oriented graphite (002)	
Scan mode		ω	
Recording range 2θ (°)		2–80	
hkl range		$0 \le h \le 36 \quad -6 \le k \le 6$ $-16 \le l \le 15$	
No. of measured reflections		3980	
Data reduction			
No. of independent reflections		2164	
$R_{int} = \sum\|I - I_{avr}\|/\sum I$		2.71%	
Absorption correction		Gaussian integration method	
Transmission coeff.		0.39–0.74	
Independant reflections with $I > 3.0\ \sigma(I)$		1404	
Refinement[a]			
Refinement		F	
F_{000}		1118	
Weighting scheme		$w = 1/[\sigma^2\|F_o\| + (0.015\|F_o\|)^2]$	
R (%)		2.57%	
R_w (%)		2.79%	
No. of refined parameters		47	
Difference Fourier residues		$[-1.45, +2.03]$ e$^-$/Å^3	
Secondary extinction		0.004(1)	

[a] $R = \sum||F_o| - |F_c||/\sum|F_o|$. $R_w = [\sum w(|F_o| - |F_c|)^2/\ \sum w|F_o|^2]^{1/2}$. Isotropic secondary extinction—Type I—Gaussian distribution (8).

2. COMPUTATIONAL ASPECTS

Self-consistent *ab initio* band structure for hollandite $Rb_{0.73}Cr_5Te_8$ (3) and pseudo-hollandite $Rb_{0.62}Cr_5Te_8$ (this work) were performed with the tight-binding linear-muffin-tin-orbital method in the atomic sphere approximation (TB-LMTO-ASA) (9). Exchange and correlation were treated in the local spin density approximation (10). All the relativistic effects except spin–orbit coupling were taken into account using the scalar relativistic approximation (11).

TABLE 2
Refined Coordinates, Atomic Displacement Parameters (ADP), and Their Estimated Standard Deviations for $Rb_{0.62}Cr_5Te_8$

Atom	x	y	z	B_{eq}[a]	τ (%)
Rb	0	0	0	3.54(8)	0.619(6)
Cr1	0	0.5	0.5	0.84(3)	
Cr2	0.20435(5)	0	0.83080(11)	0.88(2)	
Cr3	0.84084(5)	0	0.50875(12)	0.94(2)	
Te1	0.33050(2)	0	0.00496(5)	0.898(8)	
Te2	0.74193(2)	0	0.65995(5)	0.803(8)	
Te3	0.41222(2)	0	0.67327(5)	0.976(9)	
Te4	0.07243(2)	0	0.66546(5)	0.876(8)	

	U_{11}[b]	U_{22}	U_{33}	U_{13}
Rb	0.0358(12)	0.075(2)	0.0214(11)	0.0031(9)
Cr1	0.0093(5)	0.0090(6)	0.0128(6)	0.0011(5)
Cr2	0.0106(4)	0.0107(5)	0.0120(4)	0.0021(3)
Cr3	0.0112(4)	0.0108(4)	0.0142(4)	0.0037(4)
Te1	0.0113(2)	0.0106(2)	0.0120(2)	0.00247(12)
Te2	0.01060(14)	0.0084(2)	0.0122(2)	0.00406(12)
Te3	0.0115(2)	0.0116(2)	0.0138(2)	0.00297(14)
Te4	0.0088(2)	0.0098(2)	0.0135(2)	0.00050(13)

[a] Isotropic equivalent ADP defined as $B_{eq}(\text{Å}^2) = 4/3\,\text{trace}(\beta\mathbf{g})$ or $B_{eq} = (8\pi^2/3)\ \sum_i \sum_j U_{ij}|\mathbf{a}_i^*||\mathbf{a}_j^*|\mathbf{a}_i \cdot \mathbf{a}_j$.

[b] The expression of the harmonic displacement factor is $\exp(-2\pi^2 \sum_i \sum_j U_{ij}|\mathbf{a}_i^*||\mathbf{a}_j^*|h_i h_j)$, with U_{ij} in Å^2 ($U_{12} = U_{23} = 0$).

In the ASA, one assumes that the space can be filled with small overlapping Wigner–Seitz (WS) atomic spheres. The potential symmetry is considered spherical inside the spheres; a combined correction is used to take into account the overlapping part. The radii of the WS spheres were determined by the condition that the overlapping potential be the best possible approximation to the full potential. They were found by an automatic procedure described in Ref. (13). However, as the kinetic-energy error introduced by the combined correction is proportional to the 4th power of the relative sphere overlap, this overlap should not be too large. Indeed, since the structures of the compounds under study are not closely packed, the interatomic spaces were filled with interstitial spheres. The optimal positions and radii of theses additional "empty spheres" (ES) were determined by an automatic procedure also described in Ref. (13). In total, 14 (12) non-symmetry-related ES with $0.60 \leq r_{ES} \leq 1.24$ Å ($0.68 \leq r_{ES} \leq 1.27$ Å) were introduced for hollandite (pseudo-hollandite) $RbCr_5Te_8$. In this way, the maximum relative overlap between two adjacent atomic spheres was reasonable ($< 16\%$). The positions and radii of the WS are given in Table 3.

The basis set consisted of the Rb 5*s*, 5*p*, 4*d*, and 4*f*, Cr 4*s*, 4*p*, and 3*d*, Te 5*s*, 5*p*, 5*d*, and 4*f*, and, depending of the size of the spheres, ES *s*, *p*, and *d* or *s* and *p* LMTOs. The Rb 5*p*, 4*d*, and 4*f*, Te 5*d* and 4*f*, and ES *p* and d partial waves were

TABLE 3
Atomic Parameters Used for the TB-LMTO-ASA Calculations

$Rb_{0.73}Cr_5Te_8$					$Rb_{0.62}Cr_5Te_8$				
Atom	x	y	z	Radius	Atom	x	y	z	Radius
Rb	1/2	0	1/2	2.20	Rb	0	0	0	2.186
Cr1	0	0	0	1.51	Cr1	1/2	0	1/2	1.472
Cr2	0.33430	0	0.00770	1.49	Cr2	0.20435	0	0.83080	1.471
Cr3	0.81550	0	0.66810	1.46	Cr3	0.84084	0	0.50875	1.463
Te1	0.80249	0	0.84446	1.65	Te1	0.33050	0	0.00496	1.656
Te2	0.53520	0	0.17035	1.68	Te2	0.74193	0	0.65995	1.739
Te3	0.13275	0	0.83018	1.65	Te3	0.41222	0	0.67327	1.665
Te4	0.17290	0	0.50742	1.66	Te4	0.07243	0	0.66546	1.672
E1	0.18750	0	0.70833	1.24	E1	0.45833	0	0.20081	1.275
E2	0.02083	0	0.25000	1.09	E2	0.14583	0	0.15519	1.233
E3	0.43750	0	0.62500	1.09	E3	0.31250	0	0.75403	1.099
E4	0.27083	0	0.08333	1.08	E4	0.22917	0	0.08166	1.091
E5	0.39583	0	0.91667	1.03	E5	0.37500	0	0.36405	1.007
E6	0.33333	0	0.58333	0.946	E6	0.04167	0	0.42192	0.995
E7	0.43750	0	0.25000	0.877	E7	0.12500	0	0.92171	0.912
E8	0.31250	0	0.75000	0.821	E8	0.27083	0	0.57813	0.888
E9	0.08333	0	0.91667	0.783	E9	0.41667	0	0.89449	0.788
E10	0.33333	0	0.41667	0.705	E10	0.08333	0	0.25204	0.732
E11	0.01462	0.16339	0.35929	0.733	E11	0.33333	0	0.21879	0.699
E12	0.33035	0.15924	0.23429	0.702	E12	0.00955	0.15947	0.26314	0.685
E13	0.03692	0.31233	0.79236	0.636					
E14	0.12804	0.25660	0.18079	0.602					

treated by the Löwdin downfolding technique (14). The **k**-space integrations were performed with the tetrahedron method (15). The self-consistent charge density was obtained with 554 irreducible **k**-points neglecting the contribution of the nonspherical part of the charge density to the potential. Both non-spin-polarized and spin-polarized calculations were performed. A basic and complete description of the TB-LMTO-ASA is given in the so called "Varenna notes" (16).

3. DISCUSSION

3.1. Crystal Structure

The crystal structure of pseudo-hollandite $Rb_{0.62}Cr_5Te_8$ can be described in an analogous fashion to that of $TlCr_5Te_8$, that is, a three-dimensional anionic lattice ($Cr_5Te_8^{x-}$) forming channels in which rubidium is found. The anionic framework is made up of regular layers of $CrTe_6$ edge-sharing octahedra, connected by "pillaring" layers containing both face- and edge-sharing octahedra. As for $TlCr_5Te_8$, these pillaring layers (*ac* plane) are not infinite in both directions of the layer plane due to the mode of connection with the regular edge-sharing layers (*ab* plane). The mode of connection can be seen in Fig. 1 with the pillaring layers, or more precisely ribbons, depicted by the shaded octahedra. Rubidium is found within the channels, in a site having a regular 10-fold coordination with bond distances within the 3.75–3.96 Å range. For comparison, the connection mode in hollandite $Rb_{0.73}Cr_5Te_8$ is also presented in Fig. 1. The main difference between the two structures is a shift of the pillaring ribbons along the *a* axis from layer to layer for pseudo-hollandite $Rb_{0.62}Cr_5Te_8$ compared to an alignment of those ribbons in hollandite $Rb_{0.73}Cr_5Te_8$. This leads to two different cationic environments for chromium as depicted in Fig. 2, that is, a chain of two consecutive short Cr–Cr distances ($d_{Cr-Cr} = 3.068$ Å) in

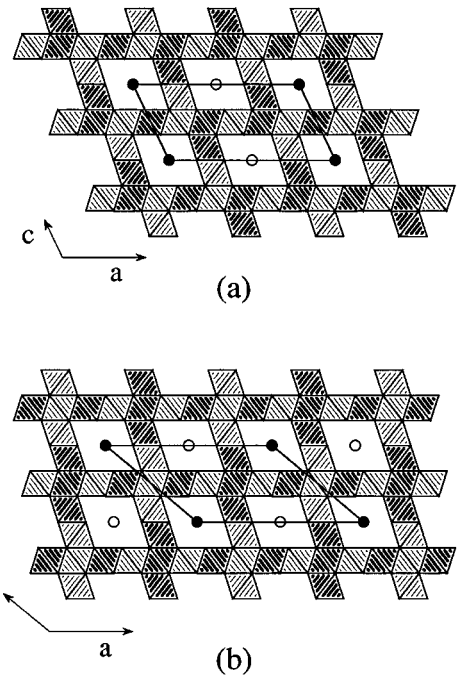

FIG. 1. Schematic view of (a) pseudo-hollandite $Rb_{0.62}Cr_5Te_8$ and (b) hollandite $Rb_{0.73}Cr_5Te_8$. Notice that face-sharing $CrTe_6$ octahedra present a similar shading. Filled and opened circles in the channels differentiate Rb atoms related by C cell centering.

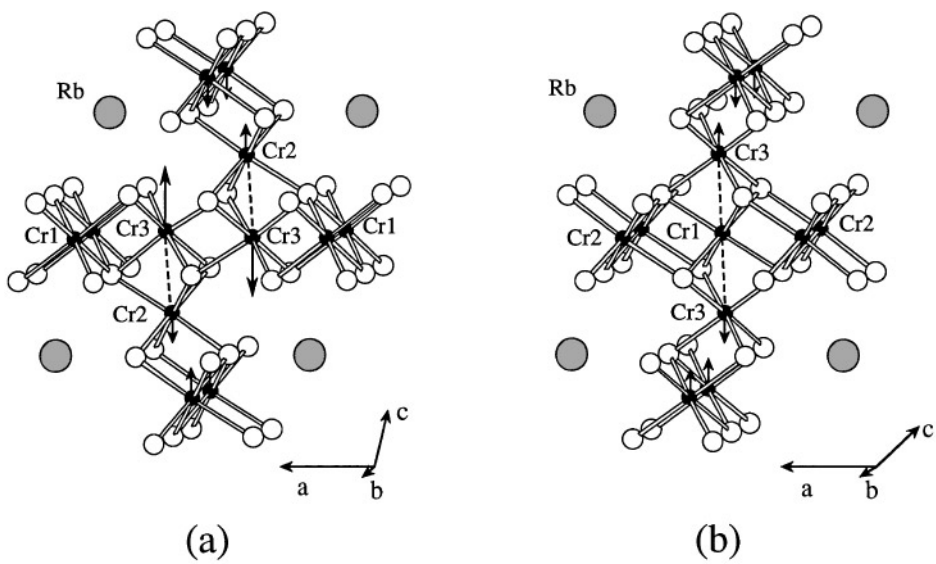

FIG. 2. Chromium environments for (a) pseudo-hollandite $Rb_{0.62}Cr_5Te_8$ and (b) hollandite $Rb_{0.73}Cr_5Te_8$. Cr off centering is indicated by arrows.

a block of three face-sharing octahedra for hollandite $Rb_{0.73}Cr_5Te_8$ and an isolated short Cr–Cr distance (d_{Cr-Cr} = 3.161 Å) between two face-sharing octahedra in pseudo-hollandite $Rb_{0.62}Cr_5Te_8$ (important interatomic distances are gathered in Table 4).

The nonstoichiometry of rubidium within these compounds is interesting and indeed $TlCr_5Te_8$ has shown similar tendencies, with large ADPs being observed at the thallium site. However the occupation of thallium, apparently, was not refined. These anomalous ADPs were assigned to a displacement of thallium within the channel, away from the origin. Anharmonic refinements of rubidium in pseudo-hollandite $Rb_{0.62}Cr_5Te_8$ (vide supra) and in hollandite $Rb_{0.73}Cr_5Te_8$ (3) have not yielded a great improvement in the Fourier difference map residues and thus the high ADPs have been demonstrated to be primarily due to a nonstoichiometry of rubidium. This nonstoichiometry will be discussed later on in this report.

Phase stability. With LMTO calculations, a comparison of stability based upon the total energy of two systems is reliable when the number of empty spheres and the atomic volume are the same for both systems and when the potential parameters are kept frozen (24). Since this is not the case in our calculations, nothing can really be concluded from total energy considerations. From our calculations we only know that the band structures of hollandite and pseudo-hollandite $RbCr_5Te_8$ are very close to each other. However, from experimental results we know that pseudo-hollandite $Rb_{0.62}Cr_5Te_8$ is slightly more stable than hollandite $Rb_{0.73}Cr_5Te_8$, the latter being obtained at higher temperatures. Since no significant difference exists between the band structures, geometric aspects have to be considered. We will see in the next section that the Cr–Cr interactions between face-sharing octahedra are globally nonbonding or weakly antibonding in nature; short Cr–Cr contacts should not, therefore, be favored. A thorough analysis of the Cr positions in the face-sharing octahedra indicates that the chromium atoms are off centered in order to increase the short Cr–Cr distances (see Fig. 2). In pseudo-hollandite $Rb_{0.62}Cr_5Te_8$, the displacement of the Cr3 atom is larger than that of Cr2 because each Cr2 sees two other Cr2 in the direction of the displacement. In hollandite $Rb_{0.73}Cr_5Te_8$, the Cr1 atoms cannot move, being at the center of the three chromium chain. Only Cr3 can be displaced, but again in a limited way because of the neighboring Cr atoms. Consequently, the Cr–Cr distance is smaller in hollandite $Rb_{0.73}Cr_5Te_8$ (d_{Cr-Cr} = 3.068 Å) than in pseudo-hollandite $Rb_{0.62}Cr_5Te_8$ (d_{Cr-Cr} = 3.161 Å). This could explain why hollandite $Rb_{0.73}Cr_5Te_8$ is less stable than pseudo-hollandite $Rb_{0.62}Cr_5Te_8$.

From the previous discussion, it can be immediately seen that there exist at least two structure types for the ternary rubidium telluro-chromates. These structures are very similar in stoichiometry and basic structural type, thus leading to materials of very similar thermodynamic stability. This similarity thus results in an inherent difficulty in determining the exact preparation conditions required for synthesis of one or the other structures. The production of the binary compound Cr_2Te_3 causes a further complication in this already complex balance between reaction products. For this reason we have been hitherto unable to carry out meaningful magnetic measurements on pure samples to determine the effect of the different chromium–chromium interactions in the different structural types and were therefore limited to theoretical investigations.

TABLE 4
Main Interatomic Distances (Å) in Pseudo-hollandite $Rb_{0.62}Cr_5Te_8$ and Hollandite $Rb_{0.73}Cr_5Te_8$

$Rb_{0.62}Cr_5Te_8$ (this work)	$Rb_{0.73}Cr_5Te_8$ (3)
$CrTe_2$ layer (*ab* plane)	
Cr1–Te3 2.7237(11) ×2	Cr1–Te1 2.7237(11) ×2
Cr1–Te4 2.7285(9) ×4	Cr1–Te2 2.7662(8) ×4
Cr3–Te2 2.761(2)	Cr2–Te1 2.726(2) ×2
Cr3–Te2 2.8135(10) ×2	Cr2–Te2 2.752(2)
Cr3–Te3 2.6971(10) ×2	Cr2–Te3 2.709(2) ×3
Cr3–Te4 2.718(2)	
Bridging Cr–Te octahedra	
Cr2–Te1 2.6950(13) ×3	Cr3–Te1 2.730(3)
Cr2–Te2 2.7765(11) ×2	Cr3–Te2 2.7748(11) ×2
Cr2–Te4 2.7605(13)	Cr3–Te4 2.695(3)
	Cr3–Te4 2.7154(11) ×2
Rb–Te	
Rb–Te1 3.9759(13) ×4	Rb–Te1 3.9760(13) ×2
Rb–Te4 3.8545(12) ×2	Rb–Te4 3.9552(12) ×4
Rb–Te3 3.7499(10) ×4	Rb–Te3 3.7409(11) ×4
Principal short Te–Te	
Te2–Te2 3.7225(11)	Te1–Te3 3.747(2)
Te4–Te4 3.7612(11)	Te1–Te2 3.7808(10)
Principal short Cr–Cr	
Cr2–Cr3 3.161(2)	Cr1–Cr3 3.0685(13) ×2

3.2. Magnetic Properties

The calculations for both allotropic forms (hollandite $Rb_{0.73}Cr_5Te_8$ and pseudo-hollandite $Rb_{0.62}Cr_5Te_8$) were done assuming a $RbCr_5Te_8$ stoichiometric composition.

Calculations without spin polarization show that the density of states (DOS) at the Fermi level is very high for the hollandite and pseudo-hollandite compounds (40.5 and 39.6 states/eV/cell, respectively). Consequently, according to the Stoner criteria (18) and in consideration of the results of the band structure calculations performed for the CrTe, Cr_3Te_4, and Cr_2Te_3 ferromagnetic compounds (1),

magnetic properties are expected for the $RbCr_5Te_8$ phases. Spin-polarized calculations have then to be considered to properly understand their band structures.

Since, up to now, no experimental magnetic data are available on the $RbCr_5Te_8$ system (vide supra), the magnetic calculations that have been carried out are based upon hypothetical magnetic structures. To build a realistic magnetic model, the competition between the direct exchange and the indirect exchange (or super exchange) has to be considered. In the case of Cr^{III} ($t_{2g}^3 e_g^0$) an antiferromagnetic coupling between the atoms is induced by a direct exchange but a ferromagnetic interaction is generated by a super exchange. Thus, the distance between the Cr atoms is critical in assessing the magnetic interaction. For edge-sharing octahedra, the super exchange is known to be the strongest effect. A ferromagnetic ordering is therefore expected in the $CrTe_2$ layer. The problem is more complicated for the coupling between two (or three) face-sharing octahedra. For such a coupling, Koneshova *et al.* reported (19) a critical Cr–Cr distance of ca. 2.98 Å, the distance observed in the Cr_2Te_3. Below this value, the exchange interactions are predominantly antiferromagnetic (Cr_3S_4, $d_{Cr-Cr} = 2.82$ Å; Cr_3Se_4, $d_{Cr-Cr} = 2.94$ Å) (20). Above this value, a ferromagnetic ordering is observed (Cr_3Te_4, $d_{Cr-Cr} = 3.09$ Å) (1). In Cr_2Te_3 no effect seems to prevail and one Cr site has a zero ordered moment (21). For the $RbCr_5Te_8$ structures, the shortest Cr–Cr distances are 3.068 Å for the hollandite type and 3.161 Å for the pseudo-hollandite type; ferromagnetic properties are thus expected (calculations with ferrimagnetic models proved this assertion to be valid).

The total DOS and Cr partial DOS obtained for pseudo-hollandite structure are presented in Fig. 3 (similar curves are obtained for the hollandite structure). The majority, spin-up direction is indicated by ↑ and the minority, spin-down direction by ↓. The assignment of the bands is straightforward. The bottom part corresponds to the low-lying Te(5*s*) bands. Then the next block is related to the Te(5*p*) and Cr(3*d*) states. From ionic considerations only, one can say that the lower part of this latter block corresponds to the Te(*p*) bands and the upper part to the Cr(*d*) bands. However, it is clear that a strong hybridization exists between the Cr(3*d*) and Te(5*p*) states. At higher energy (not shown in Fig. 3), the contributions to the DOS come from the Rb(5*s*) and Cr(4*s*) states. The states with mainly cationic 3*d* character show a clear exchange splitting. This splitting is comparable to that observed for the compounds Cr*X* (*X* = S, Se, Sb, Te) (1b). The magnetic energy (difference between the magnetic and nonmagnetic state energies) is calculated to be 3.21 eV/formula unit for the hollandite compound and 3.24 eV/formula unit for the pseudo-hollandite compound. The magnetic moments within the Wigner–Seitz spheres are gathered in the Table 5. The moments calculated for Cr (ca. 3 μ_B) correspond to the moment expected for Cr^{III}. However, the total magnetization is slightly below 15 μ_B because of the magnetic polarization of the anions.

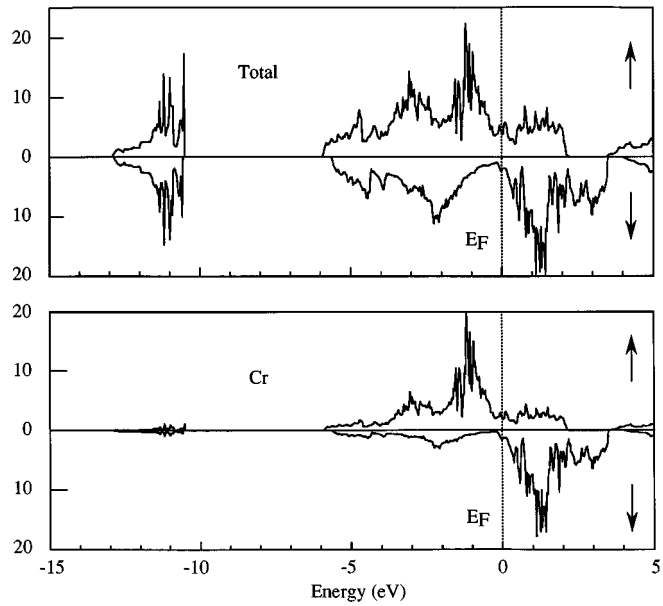

FIG. 3. Total density of states and Cr partial density of states of pseudo-hollandite $RbCr_5Te_8$ for majority (↑) and minority (↓) spin.

The effect of the Cr–Te covalence on the total magnetization is clearly visible in Fig. 4, which presents, as a function of energy, the difference between spin-up and the spin-down integrated DOS (IDOS) and Cr and Te partial IDOS. With the hybridization Scheme 1 (between the Te(*p*) states (shaded) and the Cr(*d*) states (hatched)) the Te negative magnetic polarization can be explained. When compared to the nonmagnetic case (on the left), the Te(*p*)–Cr(*d*) hybridization is increased for the spin up and decreased for the spin down, due to exchange splitting of the *d* block. As a consequence, the number of Te(*p*) states in the *d* block above E_F is higher for the spin up than for the spin down

TABLE 5
Results of Spin-Polarized Band Structure Calculations for Hollandite and Pseudo-hollandite $RbCr_5Te_8$

Moment (μ_B)	Hollandite	Pseudo-hollandite
Cr1	3.07	3.19
Cr2	3.11	3.13
Cr3	3.03	3.11
Te1	− 0.08	− 0.19
Te2	− 0.09	− 0.06
Te3	− 0.19	− 0.11
Te4	− 0.12	− 0.10
Exchange splitting (eV)	≈ 2.4	≈ 2.4
Total magnetisation (μ_B/formula unit)	14.40	14.75

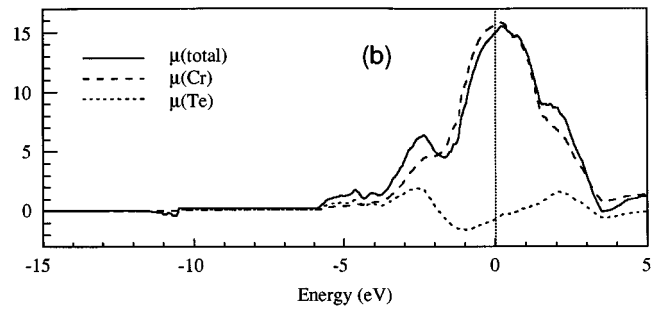

FIG. 4. Difference between the spin-up and spin-down total IDOS and Cr and Te partial IDOS for pseudo-hollandite $RbCr_5Te_8$.

TABLE 6
Te Environnement for Hollandite and Pseudo-hollandite $RbCr_5Te_8$

	Hollandite		Pseudo-hollandite	
	Nb of Cr	$\langle d_{Te-Cr}\rangle$(Å)	Nb of Cr	$\langle d_{Te-Cr}\rangle$(Å)
	4		3	
Te1	1Cr1 + 2Cr2 + 1Cr3	2.726	1Cr2 + 2Cr2 2.701	
	5		5	
Te2	2Cr1 + 1Cr2 + 2Cr3	2.768	2Cr2 + 1Cr3 + 2Cr3	2.788
	3		3	
Te3	1Cr2 + 2Cr2	2.706	1Cr1 + 2Cr3	2.708
	3		4	
Te4	1Cr3 + 2Cr3	2.708	2Cr1 + 1Cr2 + 1Cr3	2.725

and a negative magnetization appears. However, looking carefully at Table 5, a difference exists between the tellurium atoms. In fact, the smaller the number of chromium first neighbors (see Table 6), the weaker the stabilization of the Te(p) states and the larger the Cr(d)–Te(p) hybridization.

To discuss the metallic or half-metallic ferromagnetic properties of the phases (and the Rb nonstoichiometry, vide infra), one needs to know the crystalline orbital characters around the Fermi level. In Figs. 5a and 5b are plotted the spin-up (↑) and spin-down (↓) energy dispersion curves, respectively, along some high-symmetry directions of the Brillouin zone for pseudo-hollandite $RbCr_5Te_8$ (similar plots are obtained for hollandite $RbCr_5Te_8$). In both figures the Cr(d_{z^2}) (z axes along the stacking direction) contribution is emphasized by means of a "fat band" visualization, that is, a fattening of the energy dispersion lines proportional to the orbital characters. For the spin-down (↓) states, bonding, nonbonding, and antibonding d_{z^2}–d_{z^2} interactions exist between the Cr atoms of face-sharing octahedra and most bonding states are slightly occupied (the lowest fattened bands drop below the Fermi level; see Fig. 5b). As the Cr(d)–Te(p) hybridization is low for the minority states (vide supra), no broadening of the t_{2g} block due to π-type antibonding interactions is observed. In contrast, for the spin-up states the Cr(t_{2g})–Te(p) antibonding interactions are much stronger than in the nonmagnetic case and one fraction of these antibonding states is found above the Fermi level. In addition it seems that for those spin-up states the Cr d_{z^2}–d_{z^2} interactions are too small (the Cr–Cr distances too large) to push the antibonding states above the Fermi level (see Fig. 5a). In fact, charge calculations have shown that the Cr–Cr interactions between face-sharing octahedra are nonbonding or slightly antibonding in nature for both structures. Since no band gap could be found for either spin state, metallic properties are expected and therefore theses compounds cannot be half-metallic ferromagnets. That possibility cannot be ruled out for all $A_xCr_5X_8$ phases, however, since a gap for the minority states should be possible with lower anionic bands.

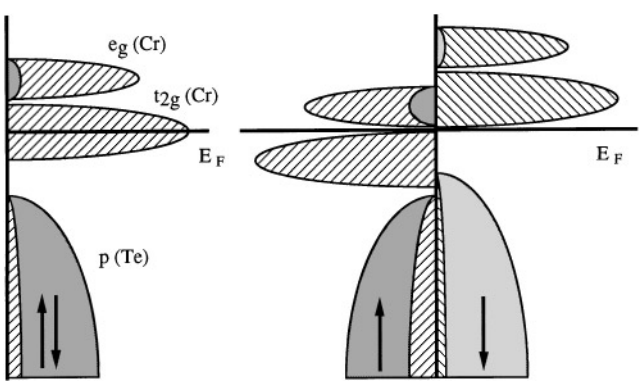

SCHEME 1

Rb nonstoichiometry. An interesting common feature of both $Rb_xCr_5Te_8$ phases is the rubidium nonstoichiometry. Within a rigid band model, taking into account such a rubidium nonstoichiometry corresponds to a removal of few electrons, that is, a lowering of the Fermi level. Considering the calculated DOS amplitude at the Fermi level, the expected shift is small (ca. 50 meV) for both compounds. Consequently, to get significant results the accuracy around the Fermi energy had to be increased. New calculations were then carried out in the following way: As the LMTO method is a linear method, the Ev values used for the linearization procedure were fixed to the Fermi energy and new sets of potential parameters were calculated (22). These potential parameters were then used to obtained an improved DOS around the Fermi level. The resulting total DOS and the DOS for both spins around the Fermi level are plotted in Fig. 6 for hollandite $RbCr_5Te_8$ (upper) and pseudo-hollandite $RbCr_5Te_8$ (lower). For both compounds, the spin-down DOS is rather small and nearly flat in the vicinity of Fermi energy. In contrast, the spin-up DOS is more important and exhibits several local maxima and minima near E_F. Therefore, a change in the Fermi level

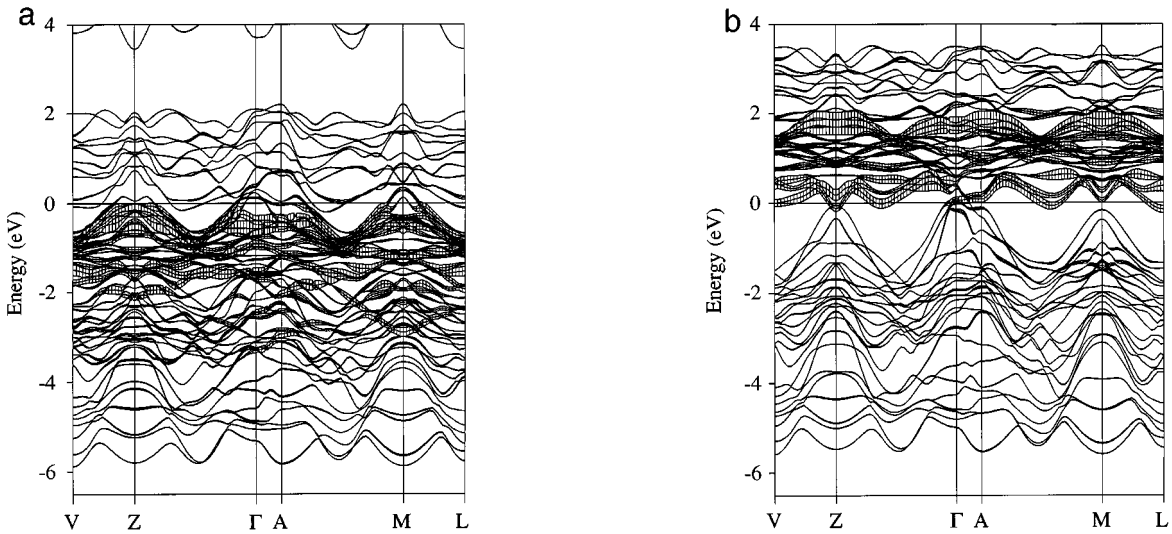

FIG. 5. Energy band dispersion of (a) majority (↑) states and (b) minority (↓) states for pseudo-hollandite $RbCr_5Te_8$. In both figures the Cr2 and Cr3 d_{z^2} contribution are projected as fat bands (with a 100% character corresponding to a line width of 0.525 eV). Symmetry points (Γ(0,0,0), A(0,0, − 1/2), Z(− 1/2,1/2,0), M(− 1/2,1/2, − 1/2), L(0,1/2, − 1/2), and V(0,1/2,0)) taken according to Ref. (17).

position generates larger changes in the spin-up structure than in the spin-down structure.

Taking into account the accuracy of the LMTO method ($\approx$10 meV for the band position), we can only give a qualitative explanation of the nonstoichiometry. For both structures, removing a few electrons will mainly reduce the population of the top of the t_{2g} majority band (see Scheme 1), that is, empty primarily π-type antibonding Cr(t_{2g})–Te(p) states (vide supra). Hence, the Cr–Te bonding will be reinforced in nonstoichiometric $Rb_xCr_5Te_8$. However, the electron removal will also deplete the bottom of the t_{2g} minority band and consequently partially reduce the Cr d_{z^2}–d_{z^2} bonding interaction. In the $Rb_xCr_5Te_8$ phases, a subtle balance should then exist between the Madelung energy, the strength of the Cr–Te bonding, and the bonding/nonbonding character of Cr–Cr interactions. It would be interesting to determine other hollandite or the pseudo-hollandite $Rb_xCr_5Te_8$ structures, seeking different x values, to see if a range of stability could exist.

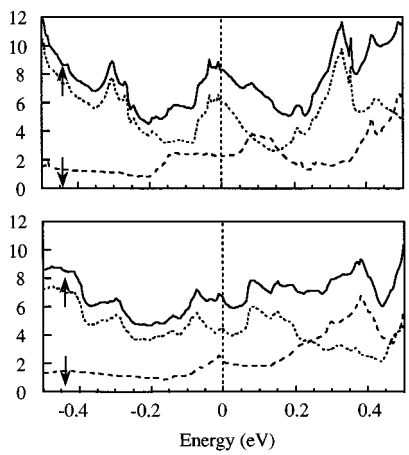

FIG. 6. Total density of states and the spin-up and spin-down partial density of states around the Fermi level for hollandite $RbCr_5Te_8$ (upper part) and pseudo-hollandite $RbCr_5Te_8$ (lower part).

4. CONCLUDING REMARKS

Pseudo-hollandite $Rb_{0.62}Cr_5Te_8$ could be obtained as single crystals and its structure refined at room temperature from X-ray diffraction data. It was shown to be analogous to the material obtained, but not fully characterized, via ion exchange of the thallium compound $TlCr_5Te_8$ and different from the hollandite form, $Rb_{0.73}Cr_5Te_8$, previously found. The nonstoichiometry of the alkali metal, also found in hollandite $Rb_{0.73}Cr_5Te_8$, is clearly demonstrated and the question of truly stoichiometric AM_5X_8 materials can be raised. Magnetic measurements or neutron diffraction experiments could not carried out since neither hollandite $Rb_{0.73}Cr_5Te_8$ nor pseudo-hollandite $Rb_{0.62}Cr_5Te_8$ could be obtained as pure phases. Nevertheless, simple deductions from the crystal structure and previous studies suggested ferromagnetic properties. With that assumption, spin-polarized band structure calculation could be carried out and the results exclude the possibility for the $Rb_xCr_5Te_8$ phases to be half-metallic ferromagnets. A lowering of the anionic bands could, however, open the gap in the minority state and give rise to such a property. Preliminary calculations on $RbCr_5Se_8$ (4i) seem to support that idea.

REFERENCES

1. (a) J. Dijkstra, H. H. Weitering, C. F. van Bruggen, C. Haas, and R. A. de Groot, *J. Phys. Condens. Matter* **1,** 9141 (1989); (b) J. Dijkstra, C. F. van Bruggen, C. Haas, and R. A. de Groot, *J. Phys. Condens. Matter* **1,** 9163 (1989). [see references therein]
2. (a) J. Dijkstra, C. F. van Bruggen, C. Haas, and R. A. de Groot, *Phys. Rev.* B **40,** 7973 (1989); (b) R. A. de Groot, F. M. Mueller, P. G. van Engen, and K. H. J. Buschow, *Phys. Rev. Lett.* **50,** 2024 (1983); (c) C. M. Fang, P. R. Tolsma, C. F. van Bruggen, R. A. de Groot, G. A. Wiegers, and C. Haas, *J. Phys. Condens. Matter* **8,** 4381 (1996).
3. J. Gareh, F. Boucher, M. Evain, C. J. O'Connor, and S. Li, *J. Solid State Chem.* **122,** 41 (1996).
4. (a) L. Fournès, M. Vlasse, and M. Saux, *Mater. Res. Bull.* **12,** 1 (1977); (b) Von J. Huster, *J. Anorg. Allg. Chem.* **447,** 89 (1978); (c) K. Klepp and H. Boller, *J. Solid State Chem.* **48,** 388 (1983); (d) W. Schramm, R. Schöllhorn, H. Eckert, and W. Müller-Warmuth, *Mater. Res. Bull.* **18,** 1283 (1983); (e) K.D. Bronsema, R. Jansen, and G.A. Weigers, *Mater. Res. Bull.* **19,** 555 (1984); (f) T. Ohtani and S. Onoue, *J. Solid State Chem.* **54,** 324 (1985); (g) T. Ohtani and S. Onoue, *Mater. Res. Bull.* **21,** 69 (1986); (h) R. Quint and H. Boller, *Mater. Res. Bull.* **22,** 1499 (1987); (i) W. Bronger, C. Herudek, J. Huster, and D. Schmitz, *Z. Anorg. Allg. Chem.* **619,** 243 (1993); (j) T. Ohtani, Y. Sano, K. Kodama, and S. Onoue, *Mater. Res. Bull.* **28,** 501 (1993); (k) T. Novet, M. Wagner, M. Jiang, and D.C. Johnson, *Mater. Res. Bull.* **30**(1), 65 (1995); (l) H. Boller, K.O. Klepp, and K. Kirchmayr, *Mater. Res. Bull.* **30**(3), 365 (1995).
5. P. J. Becker and P. Coppens, *Acta Crystallogr. A* **30,** 129 (1974).
6. S. R. Hall, H. D. Flack, and J. M. Stewart (Eds.), "XTAL3.2 Reference Manual." Univs. of Western Australia, Australia, Geneva, and Maryland, 1992.
7. V. Petříček, "SDS95 Program." Institute of Physics, Praha, Czech Republic, 1995.
8. (a) D. T. Cromer and T. J. Waber, *in* "International Tables for X-Ray Crystallography" (J. A. Ibers and W.C. Hamilton, Eds.), Vol. IV, p. 72. Kynock Press, Birmingham, England, 1974; (b) D.T.Cromer, *in* "International Tables for X-Ray Crystallography" (J. A. Ibers and W.C. Hamilton, Eds.), Vol. IV, p. 149. Kynock Press, Birmingham, England, 1974.
9. O. K. Andersen and O. Jepsen, *Phys. Rev. Lett.* **53,** 2571 (1984). [see references therein]
10. U. von Barth and L. Hedin, *J. Phys. C* **5,** 1629 (1972).
11. (a) D. D. Koelling and B. N. Harmon, *J. Phys. C* **10,** 3107 (1977); (b) H. Gollisch and L. Fritsche, *Phys. Stat. Sol. B* **86,** 145 (1978); (c) T. Takeda, *Z. Physik B* **32,** 43 (1978).
12. O. K. Andersen, O. Jepsen, and M. Sob, *in* "Electronic Band Structure and Its Applications" (M. Yussouf, Ed.), p. 1. Springer-Verlag, Berlin, 1986.
13. O. Jepsen and O. K. Andersen, *Z. Phys. B* **97,** 35 (1995).
14. W. R. L. Lambrecht and O. K. Andersen, *Phys. Rev. B* **34,** 2439 (1986).
15. P. E. Blöchl, O. Jepsen, and O. K. Andersen, *Phys. Rev. B* **49,** 16223 (1994).
16. O. K. Andersen, O. Jepsen, and D. Glötzel, *in* "Highlights of Condensed-Matter Theory" (F. Bassani, F. Fumi, and M. P. Tosi, Eds.), p. 59. North-Holland, New York, 1985.
17. C. J. Bradley and A. P. Cracknell, "The Mathematical Theory of Symmetry in Solids," Clarendon, Oxford, 1972.
18. E. C. Stoner, *Proc. R. Soc. London* **165,** 372 (1938).
19. T. I. Koneshova, K. V. Eremin, and V. M. Novotvortsev, *Inorg. Mater.* **31,** 1385 (1995).
20. J. B. Goodenough, "Magnetism and the Chemical Bond," Interscience, New York, 1963.
21. A. F. Andresen, *Acta Chem. Scand.* **17,** 1335 (1963).
22. O. Jepsen, private communication.